Jeremy R. Gulley, Sebastian W. Winkler and William M. Dennis, " Simulation and analysis of ultrafast-laser-pulse-induced plasma generation in dielectric materials," Enabling Photonics Technologies for Defense, Security, and Aerospace Applications III, Michael J. Hayduk and Andrew R. Pirich and Peter J. Delfyett and Jr. and Eric J. Donkor and John P. Barrios and Rebecca J. Bussjager and Michael L. Fanto and Robert L. Kaminski and Guifang Li and Hooman Mohseni and Edward W. Taylor, Editors, Proc. SPIE 6572, 65720R (2007).

http://dx.doi.org/10.1117/12.719464

Simulation and Analysis of Ultrafast Laser Pulse Induced Plasma Generation in Dielectric Materials

Jeremy R. Gulley, Sebastian W. Winkler, and William M. Dennis

Department of Physics and Astronomy, University of Georgia, Athens, GA 30602, USA

ABSTRACT

Recent experiments on optical damage by ultrashort laser pulses have demonstrated that the temporal pulse-shape can dramatically influence plasma generation in fused silica and sapphire. In this work a modified 3+1D nonlinear Schrödinger equation for the pulse propagation coupled to a rate equation for the plasma density in the dielectric material is used to simulate pulse propagation and plasma formation in a range of dielectric materials. We use these simulations to analyze the influence of pulse-width, pulse-shape and beam geometry on the formation of the electron plasma and hence damage in the bulk material. In particular, when possible, we simulate the effect of pulses reconstructed from experimental data. It is expected that a better understanding of the dynamics of laser-induced plasma generation will enable the accurate simulation of optical damage in a variety of dielectrics, ultimately leading to an enhanced control of optical damage to real materials and optical devices.

Keywords: Plasma Generation, Ultrafast Pulse Propagation, Nonlinear Optics, Laser-induced Damage, Fused Silica, Nonlinear Schrödinger Equation, Computational Optics.

1. INTRODUCTION

Over the past decade there has been a significant increase in the demand for methodologies for accurate and reproducible modification of materials on both the micrometer and nanometer length scales.[1–6] In particular it is desirable to effect modifications to a given material's optical properties, *e.g.* through the creation of waveguide[7] or grating structures,[8] while avoiding the onset of irreversible permanent damage.[1] High intensity, ultrafast laser pulses are now finding use in micro-machining and nanostructuring applications because of the ability to make precise material modifications both on the surface and in the bulk, without causing permanent damage to the material.[9] The widespread use of ultrashort pulses for this purpose necessitates developing a more detailed and fundamental understanding of the physical processes leading to such modification and damage on the sub-picosecond time scale.[10,11] Ultimately, this must involve a systematic investigation of the coupling between high intensity ultrashort pulse propagation and the generation of free carrier plasmas within the material.[8,12] Although there have been extensive experimental studies on plasma generation due to multiple-pulse exposure, it is notable that computer simulations of multi-pulse effects have been much more limited.[6,9,13,14]

The development of general and widely applicable models for ultrafast laser pulse induced plasma generation has been addressed by numerous authors.[5,8,10–12,15–26] To date, many authors have used cylindrically symmetric, single pulse (2+1D) simulations of laser pulse propagation both for comparison with experimental results and to develop a more general understanding of ultrafast optical damage.[8] The ubiquity of 2+1D simulations is understandable considering the computational, memory and storage requirements necessary to simulate the propagation of complex, three-dimensional fields which can undergo significant phase and structural distortion due to nonlinear effects. However, the case for running simulations with more complicated beam structures and pulse shapes has already been made by several authors.[27,28] With continuing advances computational hardware, there is good reason to expect that fully three-dimensional pulse (*i.e.* 3+1D) simulations will play an increasing role in providing a more realistic comparison with experimental results, particularly in cases where it is important to accurately determine damage thresholds for asymmetrical beams and pulses. In this work we have used three spatial plus one time dimension (3+1D) pulse propagation simulations to explore the effects of double-pulse sequences and asymmetrical beam profiles on plasma generation in fused silica. These simulations were

Further author information: (Send correspondence to W.M.D.)
W.M.D.: E-mail: bill@physast.uga.edu, Telephone: 1 706 542 2485

performed with over a range of pulse energies with particular emphasis on determining the effect of the both the spatial beam profile and the temporal pulse shape on the critical fluence as suggested by recent work in the literature.[5, 21, 29]

2. COMPUTER SIMULATIONS OF ULTRAFAST PULSE PROPAGATION AND PLASMA GENERATION IN FUSED SILICA

The electric field of a linearly polarized laser pulse can be expressed in terms of a slowly varying, complex envelope function $A(x, y, z, t)$,[30] *i.e.*

$$\vec{E}(x, y, z, t) = \frac{1}{2}\left(A(x, y, z, t)\exp\left[i\left(kz - \omega_0 t\right)\right] + \text{c.c.}\right)\hat{x}, \tag{1}$$

where k is the magnitude of the wavevector, ω_0 is the carrier frequency and the the axis of propagation is taken to be the z-axis. The intensity, $I = \frac{1}{2}n_0 c_0 \epsilon_0 |A|^2$, is given in terms of the pulse envelope function, where n_0 is the linear index of refraction, c_0 is the speed of light in a vacuum, and ϵ_0 is the permitivity of free space.

The evolution of ultrafast pulses along the propagation axis may be described by a nonlinear Schrödinger equation (NLSE) that has been modified to include free carrier plasma generation.[24]

$$\frac{\partial A}{\partial z} = i\frac{1}{2k}\nabla_{\mathrm{T}}^2 A - i\frac{k_2}{2}\frac{\partial^2 A}{\partial \tau^2} + i\frac{k\epsilon_0 c_0 n_2}{2}|A|^2 A - \frac{W_{\mathrm{PI}}U_0}{n_0\epsilon_0 c_0 |A|^2} - \frac{\sigma}{2}\left(1 + i\omega_0\tau_c\right)\rho A \tag{2}$$

The substitution $\tau = t - z/v_g$ represents a transformation to a frame propagating at the group velocity, v_g, of the laser pulse. The first term on the right hand side of the NLSE describes spatial diffraction ($\nabla_{\mathrm{T}}^2 = \partial_x^2 + \partial_y^2$); the second term accounts for temporal dispersion where k_2 is the group velocity dispersion (GVD) coefficient; the third term describes an instantaneous Kerr nonlinearity and n_2 is the intensity based nonlinear index of refraction. The remaining terms in the NLSE represent modifications needed to include plasma generation in the material. The first of these describes photoionization, where W_{PI} is the free electron generation rate due to photoionization and U_0 is the band gap energy. The final term represents a contribution to the complex index of refraction due to the presence of a free carrier plasma density, ρ, the nature of which is described below. The real part of this term accounts for absorption by free carriers while the imaginary part accounts for plasma defocusing. Here $\sigma = (1/n_0 c_0 \epsilon_0)[e^2\tau_c/m(1 + \omega_0^2\tau_c^2)]$ is the cross-section for inverse Bremsstrahlung absorption calculated from the Drude model; τ_c is the average electron collision time, e is the electronic charge, and m is the effective mass of the electron.

It should be noted that some authors include higher-order linear and nonlinear effects in the modified NLSE.[6, 9, 25, 31–33] These effects include, but are not limited to, delayed nonlinear response (Raman scattering), shock operators, and high-order dispersion. Such processes can have great importance at extremely high intensities or very short pulsewidths ($\ll 100$ fs). In our simulations we have deliberately avoided these regimes. When these additional effects were incorporated into the simulations described in this paper, they did not significantly change the outcome of our results; other authors have reached similar conclusions on the significance of these terms for the pulsewidth and intensity domains under consideration.[24, 25] In this work we use the simplest version of the modified NLSE that we believe accurately captures the behavior under investigation, further noting that this model has found widespread use in the literature.[6, 9, 24, 27, 29, 34]

Attempts to derive a comprehensive model of plasma generation have been made by many authors.[5, 8, 10–12, 15–26] In our simulations we use the model first developed by Stuard *et al.*[15, 16] which has been modified to include saturation of the plasma density.[6, 24] Electrons in the valance band are excited to the conduction band by either photoionization or impact ionization (avalanche) processes; relaxation to the valance band occurs through electron recombination. The time evolution of the plasma density is described by[6]

$$\frac{d\rho}{dt} = \left(W_{\mathrm{PI}} + \frac{\sigma I \rho}{(1 + m/m_e)U_{\mathrm{eff}}}\right)\left(1 - \frac{\rho}{\rho_{\max}}\right) - \frac{\rho}{\tau_r}, \tag{3}$$

where $U_{\mathrm{eff}} = (U_0 + e^2|A|^2/4m\omega_0)$ is the effective band gap which takes into account the "wiggle energy" of the a electron in an applied field, m is the electron rest mass, and τ_r is the electron recombination time. In this work

we use the Keldysh theory of photoionization of solids[26] to calculate the photoionization rate W_{PI}. Keldysh theory has been widely used to describe photoionization in fused silica and other optical glasses.[6,8–10,24,29]

In general terms the behavior predicted by Eq. 2 and Eq. 3 is as follows: seed electrons are initially generated by a highly nonlinear photoionization process, these electrons can then absorb sufficient energy from the laser pulse to undergo impact ionization and avalanche.[6] At the leading edge of the pulse (provided the plasma density is still far below saturation) the instantaneous intensity can reach a threshold value ($\sim$1 TWcm^{-2} in fused silica) where the avalanche rate will balance decay due to electron recombination. The plasma density will then experience a net gain so long as the instantaneous intensity remains above this threshold, even if the peak of the pulse has long past. Thus plasma densities can be achieved that may cause reversible or permanent modifications to the material. The work presented in this paper is concerned with exploring the details of plasma generation in the intensity regime where photoionization, avalanche, and electron recombination processes are competing for control over the plasma evolution.

In particular, computer simulations based upon the numerical integration of Eq. 2 and Eq. 3 for the pulse envelope and plasma density, respectively, were performed to investigate pulse propagation and plasma generation in fused silica. Fused silica was chosen because it is very well characterized at a wavelength of 800 nm which is easily accessed by Ti:sapphire systems and consequentially has been used for all of the simulations reported in this paper. The material parameters for fused silica that are used in our simulations are summarized in Table 1.

Parameter	*Description*	*Value*	*Units*
n_0	Linear refractive index	1.45	
k_2	GVD coefficient	361	fs^{2}W^{-1}
n_2	Nonlinear refractive index	2.48×10^{-16}	cm^{2}W^{-1}
U_0	Material band gap	9	eV
τ_c	Electron collision time	1.27	fs
m	Effective electron mass	0.5	m_e
$\rho_{\max}$	Maximum plasma density	6.6×10^{22}	cm^{-3}
τ_r	Electron recombination time	150	fs

Table 1. Simulation parameters for fused silica.[6]

Eq. 2 is integrated using a split step method with the linear diffraction and dispersion terms comprising the linear step and the remaining terms comprising the nonlinear step. The linear step is solved in the spectral-domain using a 3D fast Fourier transform[35] while the nonlinear step is solved in the time-domain using a fourth-order Runge-Kutta method.[36] Eq. 3 is solved purely in the time-domain using a fourth-order Runge-Kutta method.

All simulations presented in this paper were performed using a 256×256 spatial grid, however convergence was tested using a 512×512 spatial grid. The spatial resolution is taken to be $10w_0/256$ where w_0 is a measure of the beam width. The temporal grids used in these simulations contained either 512 or 1024 points, depending on whether one or two pulses were propagated; again, convergence was tested using higher grid sizes. For single pulse simulations, the temporal resolution was $10\tau_0/512$ where τ_0 is the $1/e^2$ width of a gaussian pulse. The pulse parameters used in our simulations were based upon the following considerations: peak powers were chosen to exceed the critical power for catastrophic self-focusing ($\sim$2.8 MW in fused silica), peak intensities were chosen exceed the threshold for electron avalanche to dominate electron recombination ($\sim$1 TWcm^{-2}), however the average fluence was chosen to remain below the theoretical single pulse threshold for permanent surface damage ($\sim$1.6 Jcm^{-2}).[6] Within these criteria, we simulate six experiments. The first set of simulations investigates the propagation of a cylindrically symmetric input pulses described by

$$A(x, y, \tau, z = 0) = A_0 \exp\left(-\frac{(x^2 + y^2)}{w_0^2} - \frac{\tau^2}{\tau_0^2}\right), \tag{4}$$

where $w_0 = 5.8$ μm, $\tau_0 = 150$ fs, and A_0 is scaled to give total pulse energies of 0.5 μJ and 1.0 μJ. The second second set of simulations investigates the propagation of a double pulse system of the same total energy and

fluence,

$$A(x,y,\tau,z=0) = A_0 \exp\left(-\frac{\left(x^2+y^2\right)}{w_0^2} - \frac{(\tau+\tau_s)^2}{\tau_0^2}\right) + A_0 \exp\left(-\frac{\left(x^2+y^2\right)}{w_0^2} - \frac{(\tau-\tau_s)^2}{\tau_0^2}\right); \tag{5}$$

in this case the pulse separation $2\tau_s$ was chosen to be 500 fs. The third set of simulations investigates the propagation of a noisy spatially asymmetric pulse that was digitally reconstructed from a laboratory measurement of the beam profile, $F(x,y)$, of a laser pulse from an amplified Ti:Sapphire laser, *i.e.*

$$A(x,y,\tau,z=0) = \frac{F(x,y)}{\sqrt{\frac{\pi}{2}}\tau_0} \exp\left(-\frac{\tau^2}{\tau_0^2}\right). \tag{6}$$

All of the above pulses were propagated through 50 μm of fused silica and the spatial and temporal evolution of the both the pulse envelope and the plasma density was recorded.

3. RESULTS AND DISCUSSION

The pulse propagation results of 0.5 μJ noisy asymmetric, 1 μJ cylindrically symmetric and 1 μJ noisy asymmetric pulses are summarized in Fig. 1. None of 0.5 μJ simulations exhibited significant pulse distortion as expected since the critical intensity $\sim$1 TW/cm^2 was not greatly exceeded.

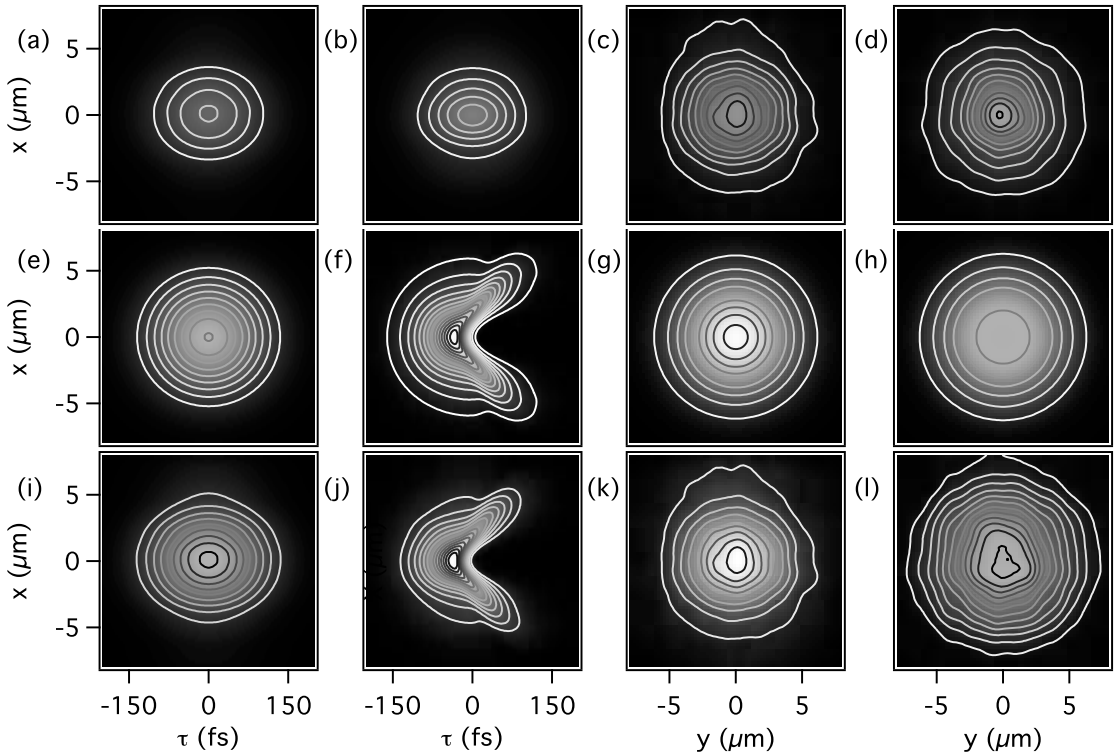

Figure 1. Noisy asymmetric pulse (0.5 μJ): Intensity profiles in the $y = 0$ plane at (a) $z = 0$ and (b) $z = 50$ μm, fluence profiles at (c) $z = 0$ and (d) $z = 50$ μm. Cylindrically symmetric pulse (1 μJ): Intensity profiles in the $y = 0$ plane at (e) $z = 0$ and (f) $z = 50$ μm, fluence profiles at (g) $z = 0$ and (h) $z = 50$ μm. Noisy asymmetric pulse (1 μJ): Intensity profiles in the $y = 0$ plane at (i) $z = 0$ and (j) $z = 50$ μm, fluence profiles at (k) $z = 0$ and (l) $z = 50$ μm.

In Fig. 1 (and also Fig. 2) the grayscale images range linearly from 0 (black) to 16 TWcm^{-2} (white) for intensity, and 0 (black) to 2 Jcm^{-2} (white) for fluence. Contour lines have also been added: for contrast these

range linearly from 1 TWcm^{-2} (white) to 16 TWcm^{-2} (black) for intensity and from 0.1 Jcm^{-2} (white) to 2 Jcm^{-2} (black) for fluence.

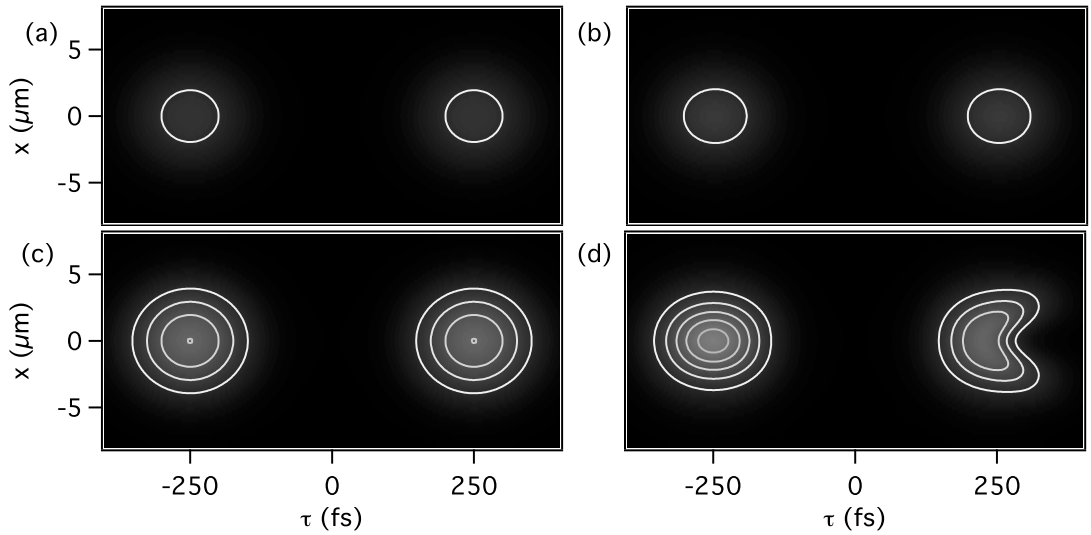

Figure 2. Cylindrically symmetric double pulse train: Intensity profiles in the $y = 0$ plane at (a) $z = 0$ and (b) $z = 50$ μm for a pulse train with total energy of 0.5 μJ. Intensity profiles at (c) $z = 0$ and (d) $z = 50$ μm for a pulse train with total energy of 1 μJ.

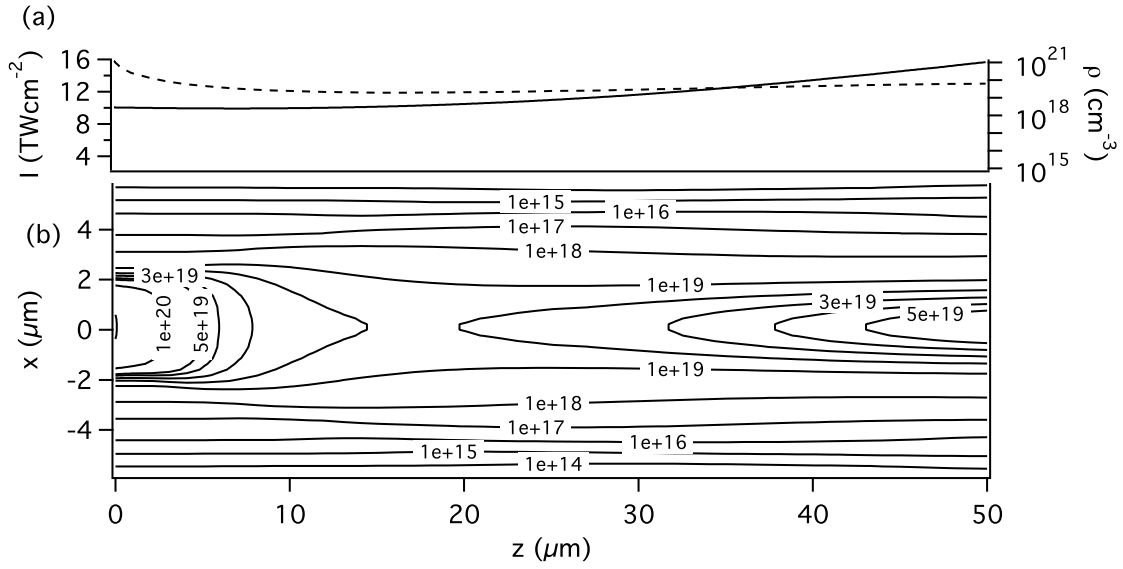

Figure 3. Single cylindrically symmetric pulse with pulse energy 1 μJ: (a) Plot of peak intensity (I, solid line) and plasma density (ρ, dashed line) as function of propagation distance. (b) Contour plot of plasma density (ρ) in the $y = 0$ plane.

For the case of the 1 μJ pulses we note that although the $y = 0$ intensity plots in Fig. 1 show only small differences the fluence plots differ noticeably between the two cases. In these simulations, the effects of plasma absorption and defocusing can clearly be seen on the trailing edge of the pulse in the intensity profiles after

propagation through 50 μm of fused silica. In Fig. 2, analogous results are shown for both 0.5 μJ and 1 μJ cylindrically symmetric double pulse simulations. Note however that the 1 μJ simulation shows minimal distortion on the front pulse but significant distortion on the trailing edge of the rear pulse after propagation through 50 μm of fused silica. Fig. 3 illustrates the variation of peak intensity and plasma density as a function of propagation distance that occurs when a 1 μJ cylindrically symmetric pulse propagates through fused silica. Simulations performed with pulse energies of 1 μJ (average fluence $\sim$1 Jcm^{-2}) all experienced an initial peak electron density on the surface of the material that was close to, but still under, the value for permanent damage in fused silica (2.2×10^{21} cm^{-3}).[24]

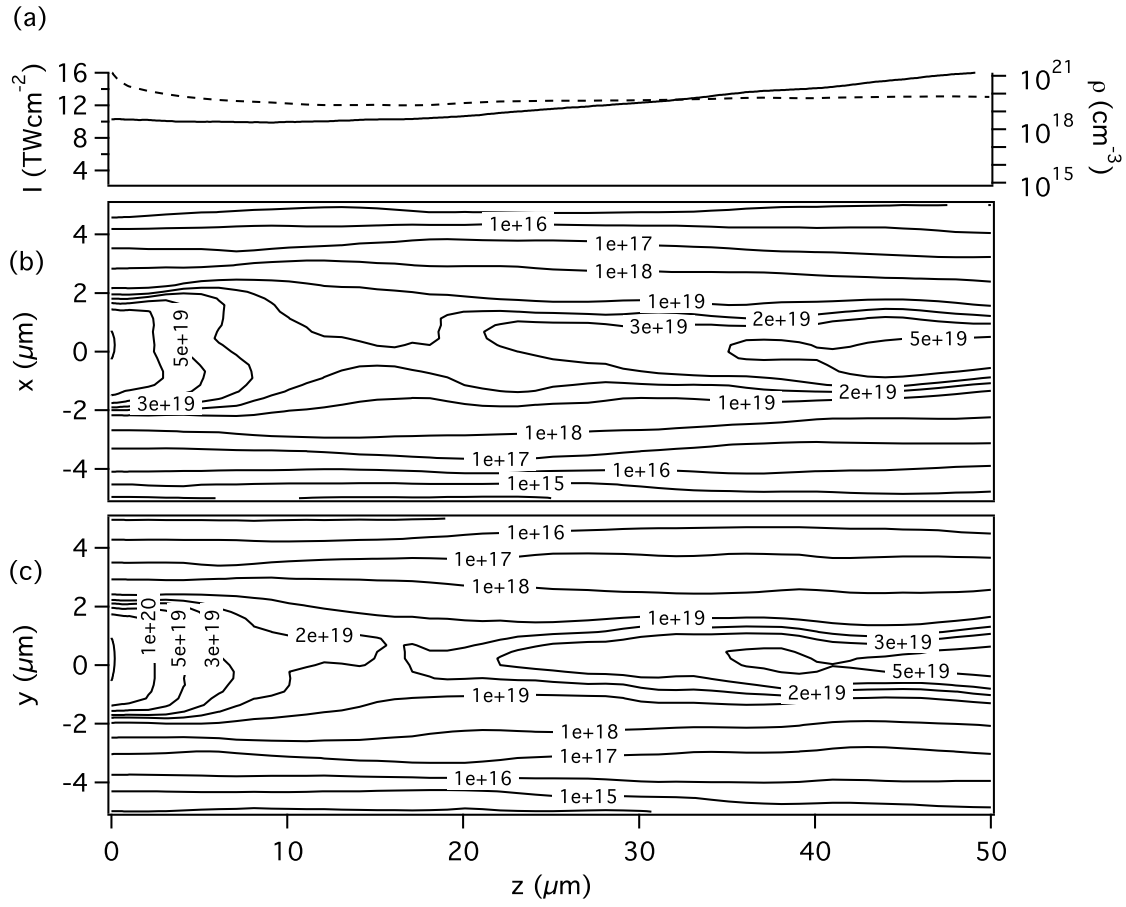

Figure 4. Single noisy asymmetric pulse with pulse energy 1 μJ: (a) Plot of peak intensity (I, solid line) and plasma density (ρ, dashed line) as function of propagation distance. (b) Contour plot of plasma density (ρ) in the $y = 0$ plane. (c) Contour plot of plasma density (ρ) in the $x = 0$ plane.

Fig. 3 shows that free carrier density declines sharply over the first 5–10 μm and then increases slowly for the remainder of the propagation; this results from self-focusing on the leading edge of the pulse as expected for pulses that exceed the critical power for catastrophic self focusing. By comparison, the 0.5 μJ simulations (not shown) exhibit a comparatively low plasma density at the beginning of the sample with little or no decrease over the first 5 μm of material; instead the peak plasma density monotonically increases as the pulses propagate through the material.

Finally, Fig. 4 illustrates the variation of peak intensity and plasma density as a function of propagation distance that occurs when a 1 μJ noisy asymmetric pulse propagates through 50 μm of fused silica. Of note is the difference between the peak plasma density contour plots from the cylindrically symmetric (Fig. 3) and

asymmetric pulses (Fig. 4). The small differences in intensity and fluence that appear in the noisy asymmetric pulse as evidenced in Fig. 1 lead to significant additional structure in the plasma channels of the material. We expect that this structure will have important implications for materials processing applications.

For comparison with fused silica, simulations were also performed in BK7 glass. For these simulations, the BK7 band gap, refractive index, and nonlinear refractive index were taken from the literature[37,38] while the remaining material parameters were set equal to those of fused silica due to a lack published data. The results from the these simulations are not presented in this paper since very similar results were obtained for the cases studied.

4. CONCLUSIONS

Simulations of ultrashort pulse propagation and plasma generation near to the damage threshold have been performed for both fused silica and BK7 glass. 3+1D simulations were performed for the cases of single, double, and noisy asymmetric pulses. For the cases of overlapping validity, the results from our simulations are in good agreement with 2+1D simulations of other authors.[6,24] We note that a comparison of the single symmetric and noisy asymmetric pulse propagation results reveals only small differences in the temporal intensity and spatial fluence profiles. However for the case of the noisy asymmetric pulse, the plasma density in the material exhibits significant structure. We attribute this behavior to the transformation of small fluctuations in the intensity into large variations in the plasma density by the highly nonlinear photoionization step. Such variations in plasma density may present a problem for researchers who wish to use ultrashort pulses precisely modify the optical properties of dielectric materials; as a consequence, future simulations will focus on a more detailed exploration of plasma generation and laser damage caused by "realistic" ultrashort pulses.

REFERENCES

1. A. Vogel, J. Noack, G. Huttman, and G. Paltauf, "Mechanisms of femtosecond laser nanosurgery of cells and tissues," *Appl. Phys. B* **81**, pp. 1015–1047, Dec 2005.
2. Y. Shimotsuma, P. G. Kazansky, J. Qiu, and K. Hirao, "Self-organized nanogratings in glass irradiated by ultrashort light pulses," *Phys. Rev. Lett.* **91**, p. 247405, Dec 2003.
3. C. B. Schaffer, A. Brodeur, J. F. Garcia, and E. Mazur, "Micromachining bulk glass by use of femtosecond laser pulses with nanojoule energy," *Opt. Lett.* **26**, pp. 93–95, Jan 2001.
4. C. B. Shaffer and E. Mazur, "Micromachining using ultrashort pulses from a laser oscillator," *Opt. and Phot. News* , pp. 20–23, April 2001.
5. X. Zhu, A. Y. Naumov, D. M. Villeneuve, and P. B. Corkum, "Influence of laser parameters and material properties on micro drilling with femtosecond laser pulses," *Appl. Phys. A* **V69**(0), pp. S367–S371, 1999.
6. S. W. Winkler, I. M. Burakov, R. Stoian, N. M. Bulgakova, A. Husakou, A. Mermillod-Blondin, A. Rosenfeld, D. Ashkenasi, and I. V. Hertel, "Transient response of dielectric materials exposed to ultrafast laser radiation," *Appl. Phys. A* **V84**(4), pp. 413–422, 2006.
7. A. Q. Wu, I. H. Chowdhury, and X. Xu, "Plasma formation in fused silica induced by loosely focused femtosecond laser pulse," *Appl. Phys. Lett.* **88**(11), p. 111502, 2006.
8. C. B. Schaffer, A. Brodeur, and E. Mazur, "Laser-induced breakdown and damage in bulk transparent materials induced by tightly focused femtosecond laser pulses," *Meas. Sci. Technol.* **12**, pp. 1784–1794, Nov 2001.
9. A. Couairon, L. Sudrie, M. Franco, B. Prade, and A. Mysyrowicz, "Filamentation and damage in fused silica induced by tightly focused femtosecond laser pulses," *Phys. Rev. B* **71**(12), p. 125435, 2005.
10. T. Q. Jia, H. Y. Sun, X. X. Li, D. H. Feng, C. B. Li, S. Z. Xu, R. X. Li, Z. Z. Xu, and H. Kuroda, "The ultrafast excitation processes in femtosecond laser-induced damage in dielectric omnidirectional reflectors," *J. Appl. Phys.* **100**, p. 023103, Jul 2006.
11. A. Rosenfeld, M. Lorenz, R. Stoian, and D. Ashkenasi, "Ultrashort-laser-pulse damage threshold of transparent materials and the role of incubation," *Appl. Phys. A* **V69**(0), pp. S373–S376, 1999.
12. B. Rethfeld, "Unified model for the free-electron avalanche in laser-irradiated dielectrics," *Phys. Rev. Lett.* **92**(18), p. 187401, 2004.

13. I. H. Chowdhury, X. Xu, and A. M. Weiner, "Ultrafast double-pulse ablation of fused silica," *Appl. Phys. Lett.* **86**(15), p. 151110, 2005.
14. O. M. Efimov, S. Juodkazis, and H. Misawa, "Intrinsic single- and multiple-pulse laser-induced damage in silicate glasses in the femtosecond-to-nanosecond region," *Phys. Rev. A* **69**(4), p. 042903, 2004.
15. B. C. Stuart, M. D. Feit, A. M. Rubenchik, B. W. Shore, and M. D. Perry, "Laser-induced damage in dielectrics with nanosecond to subpicosecond pulses," *Phys. Rev. Lett.* **74**, pp. 2248–2251, Mar 1995.
16. B. C. Stuart, M. D. Feit, S. Herman, A. M. Rubenchik, B. W. Shore, and M. D. Perry, "Nanosecond-to-femtosecond laser-induced breakdown in dielectrics," *Phys. Rev. B* **53**, pp. 1749–1761, Jan 1996.
17. J. K. Chen, D. Y. Tzou, and J. E. Beraun, "Numerical investigation of ultrashort laser damage in semiconductors," *Intern. J. Heat Mass Trans.* **48**, pp. 501–509, Jan-Feb 2005.
18. V. E. Gruzdev, "Analysis of the transparent-crystal ionization model developed by L. V. Keldysh*," *J. Opt. Technol.* **71**, pp. 504–508, Aug. 2004.
19. H. R. Reiss, "Mixed quantum and classical processes in strong fields," *Phys. Rev. A* **75**, p. 013413, Jan 2007.
20. B. Rethfeld, V. V. Temnov, K. Sokolowski-Tinten, P. Tsu, D. von der Linde, S. I. Anisimov, S. I. Ashitkov, and M. B. Agranat, "Superfast thermal melting of solids under the action of femtosecond laser pulses," *J. Opt. Technol.* **71**, pp. 348–352, Jun 2004.
21. R. E. Samad and N. D. Vieira, "Geometrical method for determining the surface damage threshold for femtosecond laser pulses," *Laser Physics* **V16**(2), pp. 336–339, 2006.
22. C. B. Shaffer, *Interaction of femtosecond laser pulses with transparent materials.* PhD thesis, Harvard University, Cambridge, Massachusetts, May 2001.
23. D. vonderLinde and H. Schuler, "Breakdown threshold and plasma formation in femtosecond laser-solid interaction," *J. Opt. Soc. Am. B* **13**, pp. 216–222, Jan 1996.
24. A. Q. Wu, I. H. Chowdhury, and X. Xu, "Femtosecond laser absorption in fused silica: Numerical and experimental investigation," *Phys. Rev. B* **72**(8), p. 085128, 2005.
25. S. Skupin and L. Berge, "Self-guiding of femtosecond light pulses in condensed media: Plasma generation versus chromatic dispersion," *Physica D* **220**, pp. 14–30, Aug 2006.
26. L. V. Keldysh, "Ionization in field of a strong electromagnetic wave," *Sov. Phys. JETP* **20**(5), p. 1307, 1965.
27. D. E. Roskey, M. Kolesik, J. V. Moloney, and E. M. Wright, "The role of linear power partitioning in beam filamentation," *Appl. Phys. B* **V86**(2), pp. 249–258, 2007.
28. V. Kudriagov, E. Gaizauskas, and V. Sirutkaitis, "Beam transformation and permanent modification in fused silica induced by femtosecond filaments," *J. Opt. Soc. Am. B* **22**, pp. 2619–2627, Dec 2005.
29. M. Mero, J. Liu, W. Rudolph, D. Ristau, and K. Starke, "Scaling laws of femtosecond laser pulse induced breakdown in oxide films," *Phys. Rev. B* **71**(11), p. 115109, 2005.
30. R. L. Sutherland, *Handbook of Nonlinear Optics*, Dekker, New York, 2nd ed., April 2003.
31. S. Tzortzakis, L. Sudrie, M. Franco, B. Prade, A. Mysyrowicz, A. Couairon, and L. Bergé, "Self-guided propagation of ultrashort ir laser pulses in fused silica," *Phys. Rev. Lett.* **87**, p. 213902, Nov 2001.
32. A. Couairon, G. Mechain, S. Tzortzakis, M. Franco, B. Lamouroux, B. Prade, and A. Mysyrowicz, "Propagation of twin laser pulses in air and concatenation of plasma strings produced by femtosecond infrared filaments," *Opt. Comm.* **225**, pp. 177–192, Sep 2003.
33. S. Skupin, G. Stibenz, L. Berge, F. Lederer, T. Sokollik, M. Schnurer, N. Zhavoronkov, and G. Steinmeyer, "Self-compression by femtosecond pulse filamentation: Experiments versus numerical simulations," *Phys. Rev. E* **74**, p. 056604, Nov 2006.
34. R. W. Boyd, *Nonlinear Optics*, Academic Press, 2nd ed., Dec. 2002.
35. M. Frigo and S. G. Johnson, "The design and implementation of FFTW3," *Proceedings of the IEEE* **93**(2), pp. 216–231, 2005. special issue on "Program Generation, Optimization, and Platform Adaptation".
36. W. H. Press, S. A. Teukolsky, W. T. Vetterling, and B. P. Flannery, *Numerical Recipes in Fortran 77*, vol. 1, Cambridge University Press, second ed., 1986.
37. D. N. Nikogosyan, *Properties of Optical and Laser-Related Materials*, John Wiley, 1997.
38. A. Horn, E. W. Kreutz, and R. Poprawe, "Ultrafast time-resolved photography of femtosecond laser induced modifications in bk7 glass and fused silica," *Appl. Phys. A* **V79**(4), pp. 923–925, 2004.